Research Article

Journal of Environmental Nanotechnology

Green Route Synthesis of Fe_3O_4 Nanoparticles and Exploring its Photochemical Activity and Antibacterial Activity

J. Manikandan[1*], P. Rajesh[2], S.V.K. Selvakumar[2]

[1]Department of Chemistry, PSG College of Arts & Science, Coimbatore, TN, India
[2]Department of Chemistry, Government Arts College, Coimbatore, TN, India
Received: 06.02.2022 Accepted: 15.02.2022 Published: 30-03-2022
*manikandan@psgcas.ac.in

ABSTRACT

Green synthesis of magnetite nanoparticles is a significantly developing methodology because of its biocompatibility. In the present work, iron oxide nanoparticles (IONPs) were synthesized by a simple Co-precipitation method using Commiphora berryi plant exudates. FTIR, XRD and SEM techniques were used to characterize the as-synthesised iron oxide nanoparticles. Photocatalytic activity of synthesized iron oxide nanoparticles was determined against Methylene blue (MB) dye in an aqueous medium. Iron oxide nanoparticles acted as a photocatalyst and decomposed the dye under solar irradiation. Results show that 73 % of degradation efficiency was attained after 150 minutes with a nanoparticle dosage of 0.5 mg/L, making the IONPs a potential applicant for various effluent treatment methods. Further, the results indicate that the efficiency increases with increasing pH and decreases with increasing MB dye concentration. The antimicrobial activity of IONPS has been studied against Escherichia coli and Staphylococcus aureus. IONPs show excellent antibacterial activity for both the organisms with 16.5 mm and 16.75 mm zone of inhibition, for *E. coli* and *S. aureus* , respectively.

Keywords: Fe_3O_4 nanoparticles; Commiphora berryi; Methylene blue; *E. coli*, and *S. aureus* .

1. INTRODUCTION

Industrial waste contains excessive hazardous materials which affect nature by water, air and soil contamination (Ghosh *et al.* 2019). Increasing environmental affairs affected humankind in this era of a fast-growing population, industrial development and macroclimate changes (Islam *et al.* 2019). Dye is a colored substance with an affinity to the material to which it is being applied like textiles, leather, plastic, etc. Dye consumption by fabric, paper, cosmetic and leather industries to color their products contributed a huge amount of dyed wastewater in the environment (Motahari *et al*. 2014). Industrial wastewater treatment requires the removal of dyes and pollutants from the effluent. Removal of dye from effluents is a demand for the good sake of the environment. In recent decades, dye degradation of industrial wastewater has become necessary to control environmental water pollution.

Nanomaterials with desired size and morphologies have drawn immense attention due to their unique morphology and size-dependent physicochemical properties and their importance in basic scientific research and potential applications (Mohapatra *et al.* 2010; Shi *et al.* 2012). Various transition metal oxide nanoparticles exhibit high chemical stability, ecofriendly nature, range of bandgap energies, good photocatalytic activity and high surface area (Nwankwo *et al*. 2019). Iron oxide nanoparticles are potential nanomaterials for applications such as MRI agents, photocatalysts and biomedical drug carriers. Due to their nano size, they become a single domain and exhibit exclusive magnetic, optical and electronic properties and they are used as an effective tool for the elimination of pollutants from wastewater and air. Methylene blue is a thiazine dye with the molecular formula $C_{16}H_{18}ClN_3S$, used in various fields. It is a dark green odorless powder; when dissolved with water, it gives the blue color solution. In the present work, *Commiphora berryi* exudates stabilized magnetite nanoparticles were synthesized by the Co-precipitation method as nano-photocatalyst. These nanoparticles were characterized by FTIR, XRD and SEM techniques and their photocatalytic efficiency was established against methylene blue dye.

2. MATERIAL AND METHODS

2.1 Materials

The chemicals ferric chloride ($FeCl_3.6H_2O$), ferrous chloride ($FeCl_2.4H_2O$), NH_4OH and hydrochloric acid (HCl) were purchased from Merck. The plant exudates were collected from *Commiphora berryi* shrub by making a deep cut on the barks.

2.2 Preparation of Iron Oxide Nanoparticles

The Iron Oxide Nanoparticles were synthesized using the procedure suggested by Arsalani *et al.* (2018) using an ethanolic solution of chosen plant exudates. Briefly, an alcoholic solution of plant exudates with 1% concentration was mixed with the NH_4OH solution in a beaker and heated to 90 °C. To the mixture, a hot solution of 60 ml Fe(II)/Fe(III) with 1:2 molar ratio was added with vigorous stirring for about 10 minutes and pH of the solution was adjusted to 11. The color change from yellowish orange to black indicates the formation of iron oxide nanoparticles. The prepared nanoparticles were separated using an external magnet, washed with doubly distilled water and dried in the oven for 1 hour at 90 °C.

2.3 Characterization of Nanoparticles

The synthesized iron oxide nanoparticles were characterized using FTIR, XRD and SEM techniques.

3. RESULTS AND DISCUSSION

3.1 FTIR Analysis

The FTIR spectra of *Commiphora berryi* exudates and *Commiphora berryi* exudates coated iron oxide nanoparticles are shown in Fig. 1. The peak at 578 cm^{-1} is the distinctive peak for the Fe-O bond, confirming the formation of Iron oxide nanoparticles (Adrian *et al*. 2019). The plant exudates may contain various phytochemicals like carbohydrates, polyphenols, phytosterols, proteins, amino acids, flavonoids and gums (Latha *et al*. 2006). The strong peak at 1030 cm^{-1} is due to the C-O bond on flavonols and the peak at 1450 cm^{-1} is due to the aromatic ring in the extract. The broadband at 3270 cm^{-1} is assigned to O–H stretching vibration of phenolic compounds and N-H stretching of amino acids (Suman *et al*. 2013).

The doublet at 2926 cm^{-1} and 2864 cm^{-1} are the vibrations of lipids present in the exudates. The band at 1640 cm^{-1} is due to N-H bending from proteins. The band at 1372 cm^{-1} is due to C–N stretching found in the proteins (Zahir *et al.* 2012) present in the plant material. The bands at 1247 cm^{-1} and 1726 cm^{-1} correspond to C-O-C stretching and C=O stretching of polysaccharides (Fahad *et al.* 2020).

3.2 X-ray Diffraction Analysis (XRD)

The XRD pattern of IONPs presented in Fig. 2 has six diffraction peaks with 2θ values of 30.56°, 35.86°, 43.48°, 53.86°, 57.63° and 62.71°, which are the peaks of the crystallographic planes: (220), (311), (400), (422), (511) and (440). The diffraction peaks in the XRD pattern correspond to the diffraction peaks of Fe_3O_4 according to JCPDS Card number 88–0315. These peaks correspond to the diffraction peaks of Fe_3O_4 nanoparticles (Tania *et al.* 2019). The synthesized iron oxide nanoparticles were figured out to be in pure crystalline form from the sharp X-ray diffraction peaks. Crystalline sizes of the IONPs were calculated using the Debye-Scherrer formula, which is found to be 14 nm.

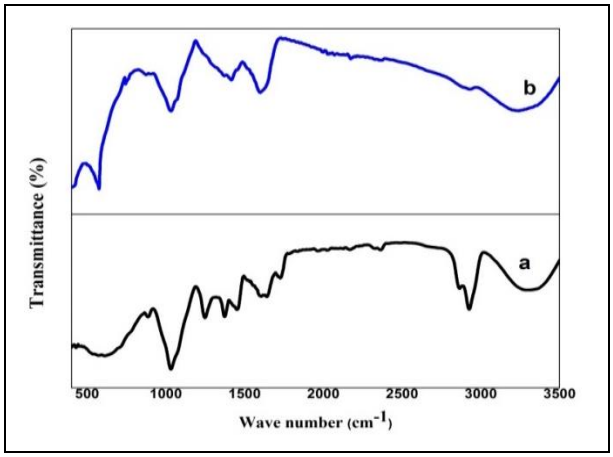

Fig. 1: FTIR spectra of (a) *Commiphora berryi* exudates and (b) *Commiphora berryi* exudates coated iron oxide nanoparticles

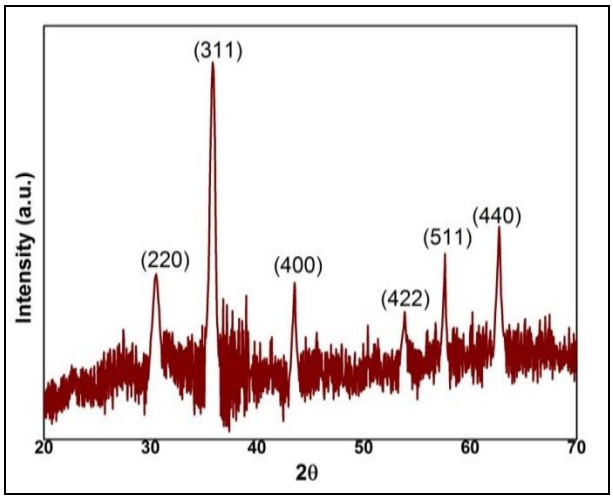

Fig. 2: X-ray diffraction pattern of CBIONPs

3.3 SEM Analysis

SEM image of IONPs in Fig. 3 exhibits well-dispersed spherical shaped nanoparticles with less particle agglomeration. The result confirms the role of plant exudates as a surfactant to control the particle aggregations.

4. PHOTOCATALYTIC ACTIVITY

To study the photocatalytic activity of nanoparticles, MB dye solution having 150 ppm concentration was prepared and taken in a 100 ml beaker with 0.5 mg/L of iron oxide nanoparticles, kept in solar light irradiation and the absorbance was measured with

different time intervals; the equation calculated the degradation efficiency of the synthesized IONPs,

$$Degradation\ efficiency\ (\%) = \frac{C_0 - C_t}{C_0} X100$$

where, C_0 - initial concentration of MB dye; C_t - concentration of MB dye at time t. The concentration of the dye at a certain time was calculated as a function of absorbance using a UV-Visible spectrophotometer. A series of experiments were carried out to find the effect of pH and the effect of dye concentration on the degradation efficiency of IONPs.

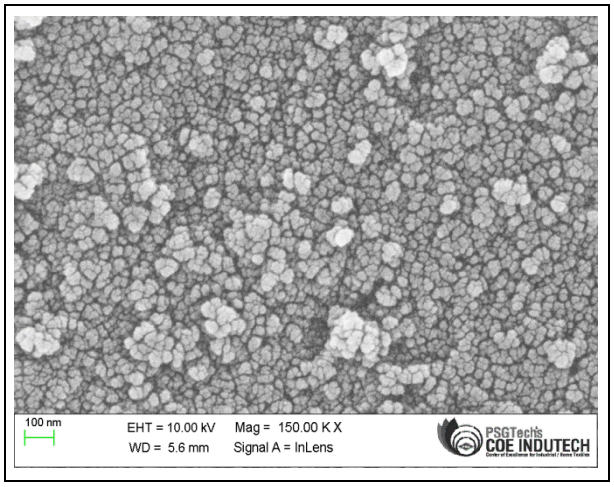

Fig. 3: SEM images of IONPs

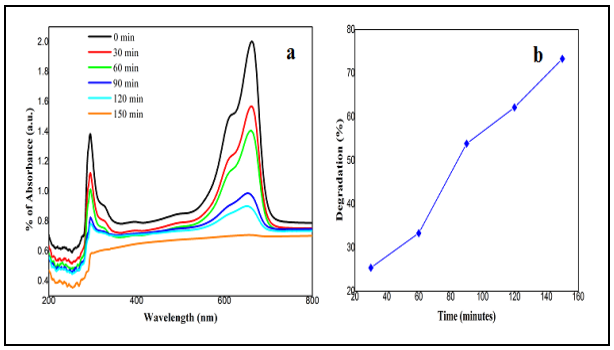

Fig. 4: (a) Degradation of MB with time and (b) Degradation efficiency of IONPS

From Fig. 4 (a), it is seen that the concentration of dye decreases by increasing the irradiation time from 0 to 150 minutes. Fig. 5(b) indicated that the degradation efficiency of IONPs increased with time and reached 73% after 150 minutes of irradiation.

The effect of pH on the degradation efficiency was a study with different pH of dye solutions ranging from 2-10. Fig. 5 shows that the highest efficiency of 98% was attained at 240 minutes for pH 10; the efficiency increased when the increase in pH value of the solution. In alkaline pH, adsorbent molecules are surrounded by negatively charged hydroxyl ions, which cause effective adsorption of positively charged MB dye molecules on the surface of iron oxide nanoparticles, enhancing the degradation (Junwang *et al*. 2005).

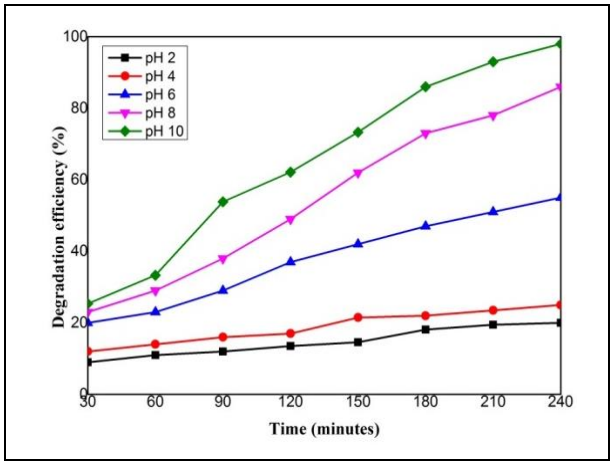

Fig. 5: Effect of pH on Degradation efficiency

In an acidic medium, the protons surrounded the adsorbent molecules repelling the positively charged MB dye from the surface of iron oxide nanoparticles, which reduces the probability of degradation.

The role of the initial concentration of MB on the degradation efficiency was studied by varying the dye concentrations as 50 ppm, 100 ppm, 150 ppm and 200 pm. For this study, the pH of the solution was fixed at 2, and 0.5 m/L concentration of IONPs has been used. Fig. 6 shows that the degradation efficiency decreases with the increasing dye dosage. 50 ppm solution reached its maximum degradation in 120 minutes and the 200 ppm solution reached the maximum degradation only in 300 minutes.

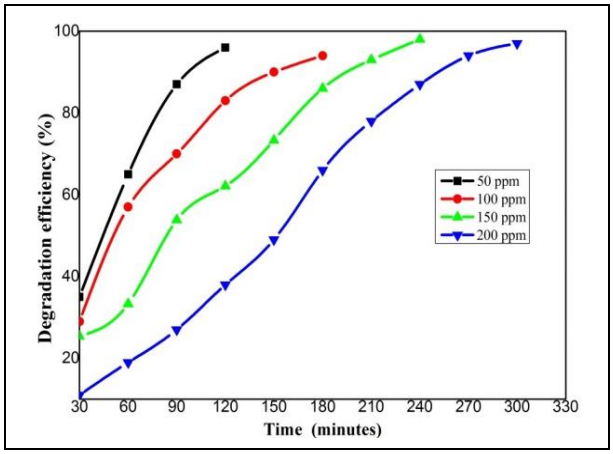

Fig. 6: Effect of irradiation time

At high concentrations, a certain amount of UV light is absorbed by the dye molecules adsorbed on the IONPs surface. Also, the MB molecules scatter the

incident light, decreasing the absorbance efficiency of nanoparticles, which decreases the degradation process.

5. ANTIBACTERIAL ACTIVITY

The medium was prepared by dissolving 2.8 g of the commercially available Nutrient Agar Medium (HiMedia) in 100 ml of distilled water. The dissolved medium was autoclaved at 15 lbs pressure at 121°C for 15 minutes. The autoclaved medium was mixed well and poured onto 100 mm Petri plates (25-30 ml/plate) while still molten. The nutrient broth was prepared by dissolving 2.8 g of commercially available nutrient medium (HiMedia) in 100 ml distilled water and boiled to dissolve the medium completely. The medium was dispensed and sterilized by autoclaving at 15 lbs pressure (121ºC) for 15 minutes.

Table 1. Zone of inhibition of IONPS

Name of the organism	Zone of inhibition (mm)				
	5 mg/ml	2.5 mg/ml	1 mg/ml	0.5 mg/ml	PC
S. aureus	16.75	12.5	9.35	5.25	17.5
E. coli	16.5	10.25	6.25	6.15	9.5

Petri plates containing 20 ml nutrient agar medium were seeded with 24-hour culture of *S. aureus* - 902 and *E. coli* - 443 bacterial strains. Wells were cut and various concentrations of IONPS (5, 2.5, 1 and 0.5 mg/ml) were added. The plates were then incubated at 37 °C for 24 hours. The antibacterial activity was assayed by measuring the diameter of the inhibition zone formed around the wells. Gentamicin antibiotic was used as a positive control and the results were shown in Fig. 7.

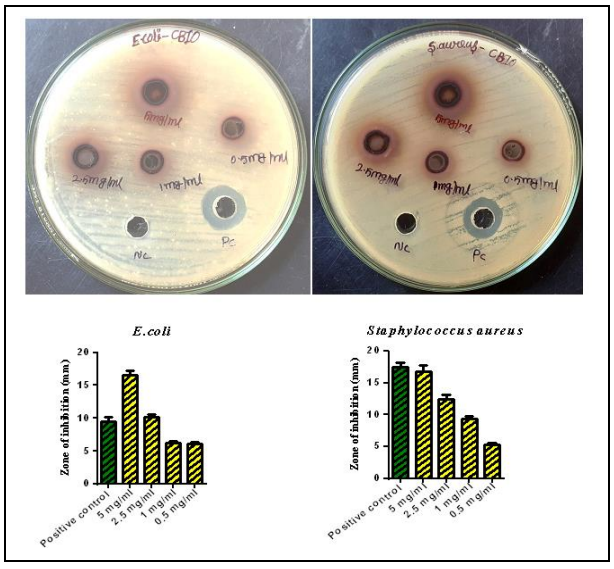

Fig. 7: Antibacterial activity of IONPs on *E. coli* and *S. aureus*

The zone of inhibition (mm) increases with the increasing concentration of iron oxide nanoparticles and the values are given in Table 1.

At the concentration of 5 mg/L, the highest inhibition is attained and the zone of inhibition (mm) is 16.5 and 16.75 for *E. coli* and *S. aureus*, respectively.

6. CONCLUSION

Iron oxide nanoparticle was synthesized through a green Co-precipitation method using *Commiphora berryi* exudates as a stabilizing and capping agent. Characterization techniques confirm the formation of iron oxide nanoparticles and the capping of plant exudates on the surface of the synthesized nanoparticles. Fe_3O_4 nanoparticles acted as efficient photocatalysts for the degradation of Methylene blue dye under solar irradiation. The degradation efficiency was measured as 73% when nanoparticle concentration is 0.5 mg/L with an irradiation time of 150 minutes. The efficiency of IONPs increases with pH and degrades maximum dye at a pH of 10. On increasing the MB dye concentration, the degradation efficiency was reduced. For 50 ppm dye, the maximum degradation was attained within 120 minutes; for 200 ppm dye solution, 97% degradation was attained after 300 minutes. Therefore, the synthesized IONPs can be used in environment-related applications such as industrial wastewater treatment; also, the iron oxide nanoparticles have potential antibacterial activity against *E. coli* and *S. aureus*.

FUNDING

This research received no specific grant from any funding agency in the public, commercial, or not-for-profit sectors.

CONFLICTS OF INTEREST

The authors declare that there is no conflict of interest.

6. REFERENCES

Adrian Radon, Patryk Włodarczyk, Aleksandra Drygała and Dariusz Łukowiec, Electrical properties of epoxy nanocomposites containing Fe_3O_4 nanoparticles and Fe_3O_4 nanoparticles deposited on the surface of electrochemically exfoliated and oxidized graphite, *Appl. Surf. Sci.*, 474, 66-77 (2019). https://doi.org/10.1016/j.apsusc.2018.05.045

Arsalani, S., Guidelli, E. J., Araujo, F.D.F., Bruno, A.C., Baffa, O., Green Synthesis and Surface Modification of Iron Oxide Nanoparticles with Enhanced Magnetization Using Natural Rubber Latex, *ACS Sustainable Chem. Eng.*, 6 (11), 13756-13765 (2018). https://doi.org/10.1021/acssuschemeng.8b01689

Fahad, M., and Alminderej, Study of new cellulosic dressing with enhanced antibacterial performance grafted with a biopolymer of chitosan and myrrh polysaccharide extract., *Arabian J. Chem.*, 13, 3672-3681 (2020). https://doi.org/10.1016/j.arabjc.2019.12.005

Ghosh, M., Manoli, K., Shen, X., Wang, J., and Ray, A.K., Solar photocatalytic degradation of caffeine with titanium dioxide and zinc oxide nanoparticles, *J. Photochem. Photobiol.* A: Chem., (377), 1-7 (2019). https://doi.org/10.1016/j.jphotochem.2019.03.029

Islam, M. A., Ali, I., Karim, S. M. A., Hossain and Firoz M. S, A.-N. Chowdhury, D.W. Morton and M.J. Angove, Removal of dye from polluted water using novel nano manganese oxidebased materials, *J. Water Process Eng.*, (32), 100911-100918 (2019). https://doi.org/10.1016/j.jwpe.2019.100911

Junwang, Tang, Zhigang, Zou, and Jinhue, Ye, Kinetics of MB degradation and effect of pH on the photocatalytic activity of MIn_2O_4 (M=Ca, Sr, Ba) under visible light irradiation, *Res. Chem. Intermed.*, 31, 513-519 (2005). https://doi.org/10.1163/1568567053956699

Latha, S., Selvamani, P., Pal, T. K., Gupta, J. K., and Ghosh, L. K., Pharmacognostical studies on leaves of *Commiphora caudata* (Wight & Arn) engl, *Ancient Sci. Life*, XXVI (1&2), 19-25 (2006).

Mahdavi, Mahnaz, Mansor Bin Ahmad, Md Jelas Haron, Farideh Namvar, Behzad Nadi, Mohamad Zaki Ab Rahman and Jamileh Amin, Synthesis, Surface Modification and Characterisation of Biocompatible Magnetic Iron Oxide Nanoparticles for Biomedical Applications, *Molecules*, 18, 7533-7548, (2013). https://doi.org/10.3390/molecules18077533

Mohapatra, M. and Anand, S., Synthesis and applications of nano-structured iron oxides/hydroxides-a review, *Int. J. Eng. Sci. Technol*, 2(8), 127-146 (2010). https://doi.org/10.4314/ijest.v2i8.63846

Motahari, F., Mozdianfard, M. R., Soofivand, F., and M. SalavatiNiasari, NiO nanostructures: synthesis, characterization and photocatalyst application in dye wastewater treatment, *RSC Adv*, 4, 27654–27660, (2014). https://doi.org/10.1039/C4RA02697G

Nwankwo, U., Bucher, R., Ekwealor, A.B.C, Khamlich, S., Maaza, M. and Ezema, F.I., Synthesis and characterizations of rutile-TiO_2 nanoparticles derived from chitin for potential photocatalytic applications, *Vacuum*, 161, 49–54 (2019). https://doi.org/10.1016/j.egyr.2020.02.010

Shi, R., Chen, G., Ma, W., Zhang, D., Qiu, G. and Liu, X., Shape-controlled synthesis and characterization of cobalt oxides hollow spheres and octahedral, *Dalton Trans*, 41, 5981-5987 (2012). https://doi.org/10.1039/C2DT12403C

Suman, T. Y., Elumalai, D., Kaleena, P.K. and Radhika, Rajasree, S., GC–MS analysis of bioactivecomponents and synthesis of silver nanoparticle using *Ammannia accifera* aerial extract and its larvicidal activity against malaria and filariasis vectors, *Ind. Crops., Prod*, 47, 239-245 (2013). https://doi.org/10.1016/j.indcrop.2013.03.010

Tania, Tofaz., Dhananjoy Chandra Mahanto, Shamima Akhter, Md. Mahbubor Rahman, M. Abdul Latif, Synthesis and Characterization of Bi-Functional Poly (Acrylic Acid-Co-2-hydroxyethylmethacrylate) Coated Iron Oxide Magnetic Composite Particles, *American J. Polymer Sci. Technol.*, 5(1), 1-8 (2019). https://doi.org/10.11648/j.ajpst.20190501.11

Zahir, A. A. and Rahuman A. A., Evaluation of different extracts and synthesised silver nanoparticles from leaves of Euphorbia prostrata against Haemaphysalis bispinosa and Hippobosca maculate, *Vet. Parasitol.*, 187, 511-520 (2012). https://doi.org/10.1016/j.vetpar.2012.02.001